Nanoscale investigation of longitudinal surface acoustic waves

Jianshu Yang, P. U. Voigt, and R. Koch[a)]
Paul-Drude-Institut für Festkörperelektronik, Hausvogteiplatz 5-7, D-10117 Berlin, Germany

(Received 18 November 2002; accepted 23 January 2003)

Scanning tunneling microscopy of longitudinally polarized surface acoustic waves (SAWs) yields amplitude and phase images with nanometer resolution. The eccentricity of the surface oscillation calculated from the experimental data by the model of Chilla *et al.* is $88° \pm 5°$ in good agreement with the macroscopic value for high velocity pseudo SAWs. Our study reveals that reliable amplitude and phase information can be deduced even from atomic scale features; however, the local surface geometry and tip shape need to be treated in more detail. © *2003 American Institute of Physics.* [DOI: 10.1063/1.1561578]

Surface acoustic waves (SAWs) are of great interest in many respects: (i) SAWs play a key role for frequency filtering in mobile phone and satellite telecommunication; (ii) SAWs are a well-established probe in materials science for material characterization[1] and quantitative determination of the elastic constants of bulk and thin films;[2] and (iii) recently SAWs have also been employed in more basic studies, e.g., to modify the electronic properties and to induce spin transport in semiconductors.[3–5] Thus, understanding the nature of acoustic wave fields, particularly of their interaction with structural features and local elasticity, is not only important for the advancement of SAW devices but also of scientific interest.

Chilla and co-workers demonstrated that scanning probe techniques—despite their large response times—are sensitive to high frequency (HF) surface acoustic wave fields ($\sim$10 MHz$\rightarrow\sim$GHz). By utilizing the unique spatial resolution of the scanning tunneling microscope (STM), amplitude and phase of Rayleigh waves were detected with nanoscale resolution,[6,7] i.e., far beyond the diffraction limit of optical detection systems.[8] Behme *et al.*[9] recently determined the phase velocity of Love waves by atomic force microscope; these SAWs exhibit a purely in-plane polarization and therefore are difficult to detect with standard techniques.

In this study we employed our UHV SAW–STM[10] to investigate high-velocity-pseudo surface acoustic waves (HVPSAWs) on Y-cut $LiNbO_3$. HVPSAWs are special types of PSAWs which are known for leaking energy into the bulk during propagation. Since HVPSAWs exhibit higher phase velocities than normal SAW modes, the operating frequency of SAW devices can be increased without necessarily decreasing the lithographical feature sizes. Compared with the well known Rayleigh waves, HVSAWs have a predominant longitudinal oscillation behavior. On Y-cut $LiNbO_3$, for instance, the component perpendicular to the surface (u_3) amounts only 3% of the in-plane component (u_1); for the correponding Rayleigh mode $u_3 \approx 1.3u_1$. Although HVPSAWs have been extensively studied theoretically in the past, very little experimental work has been devoted to them because of the difficulties involved in detecting their predominant in-plane polarization. We will show here that also the SAW–STM is sensitive to the in-plane components of the surface oscillation and that amplitude and phase information can be deduced even from atomic scale features of the surface.

The experiments presented here were performed in an UHV system consisting of separate chambers for sample preparation and SAW–STM investigation (base pressure $< 2 \times 10^{-10}$ hPa). The UHV SAW–STM—developed recently in our group[10]—is based on a commercial Omicron STM-1 and has been modified by adding a UHV-compatible high-frequency wiring system for SAW excitation and signal detection up to frequencies of 1 GHz. The substrate is a Y-cut $LiNbO_3$ piezoelectric single crystal, carrying a lithographically fabricated interdigital transducer (IDT) for exciting the HVPSAW. As confirmed by a frequency analyzer, its frequency is 210.06 MHz, i.e., well separated from the Rayleigh wave at 120 MHz. In addition, a 100-nm-thick gold film—forming the conducting layer for the SAW–STM experiments—was deposited *in situ* into the acoustic beam path of the IDT. To favor the formation of extended flat terraces we choose a substrate temperature of 400 °C and a rate of 0.1 nm/s.[11]

The experimental setup of a SAW–STM is schematically illustrated in Fig. 1. The STM tip is positioned above the conducting film on the piezoelectric sample, which is located in the propagation region of the SAW excited by the IDT on the left. The SAW-induced surface oscillations at the frequency f_{SAW} give rise to a HF contribution to the tunneling current between tip and conducting layer. The HF component is mixed at the nonlinear current–distance characteristics of the tunneling gap with a HF voltage V_{mod} at the frequency $f_{\mathrm{SAW}} + \Delta f$, which is added to the common dc tunneling voltage V_0. The mixing signal at the difference frequency Δf is chosen to be in the kilohertz range, where it can be easily analyzed by conventional STM electronics and lock-in technique. The mixing signal, which is recorded simultaneously with the topography, exhibits the amplitude and phase information of the SAW. Particularly the latter can be used to quantitatively determine the eccentricity of the SAW oscillation ellipse on areas as small as 5×5 nm (Ref. 12).

The Au film—used as a conducting layer in our tunnel-

a)Electronic mail: koch@pdi-berlin.de

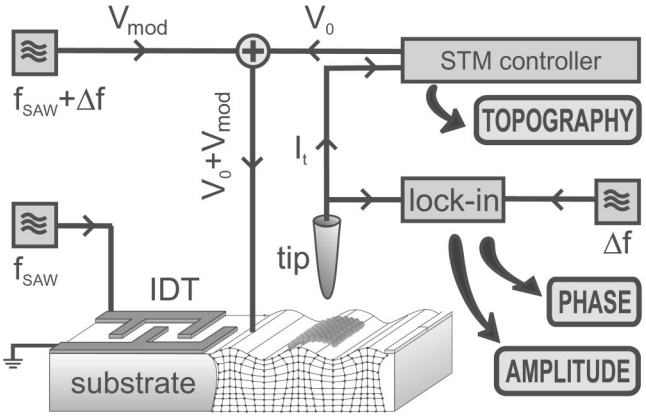

FIG. 1. Experimental setup of the SAW–STM for the measurement of SAW motion. The SAW-induced tunneling current modulation at the frequency f_{SAW} is mixed with the modulation of the tunneling voltage ($f_{SAW}+\Delta f$) at the nonlinear current–distance characteristic of the tunneling gap. A lock-in amplifier extracts the resulting difference frequency signal (Δf) yielding amplitude and phase of the SAW, which both are recorded in addition to the topography.

ing experiments—exhibits a textured morphology and consists of crystalline islands with mainly hexagonal and occasionally rectangular shapes and dimensions ranging from 10 to 150 nm. The STM topview of Fig. 2(a) shows a grain with a 30 nm wide horizontal plateau that is framed by a 2 nm high bulged border (B). The plateau consists of atomically flat extended (111) terraces separated by two steps, S_1 and S_2, of single atomic height.

While scanning the topography, also the phase and amplitude at the difference frequency are simultaneously extracted from the tunneling current. The corresponding gray-scale images, displayed in Fig. 2(b), demonstrate that SAW–STM is indeed sensitive to SAWs with negligible out-of-plane oscillation. Interestingly many details of the surface morphology can also be recognized in the two SAW-induced images, such as the plateau with two monosteps or its bulged border.

According to the model of Chilla *et al.*,[6,13] both amplitude A and phase φ of the distance modulation signal measured in the SAW–STM experiment depend on the local tilt of the surface. Since the electrons tunnel mainly along the shortest line between tip apex and sample surface, the oscillation ellipse is monitored at different stages depending on the local inclination angles γ_x and γ_y of the surface along and perpendicular to the propagation direction of the SAW [compare Fig. 3(a)]. The detected amplitude and phase modulations obviously are linked to structural features and therefore are the result of the imaging process and not due to local variations in amplitude or phase. In fact, with a wavelength of about 3.5 μm, both amplitude and phase of the excited leaky wave are essentially constant on the length scale of typical STM images ($\Delta\theta<6°$ for Fig. 2). Quantitative evaluation[6,13] yields the following equations for A and φ:

$$A = u_0 \sqrt{\frac{\sin^2\beta}{1+g_y/g_x+1/g_x} + \frac{\cos^2\beta}{1+g_x+g_y}}, \tag{1}$$

$$\varphi = \arctan(\tan\beta \ \tan\gamma_x). \tag{2}$$

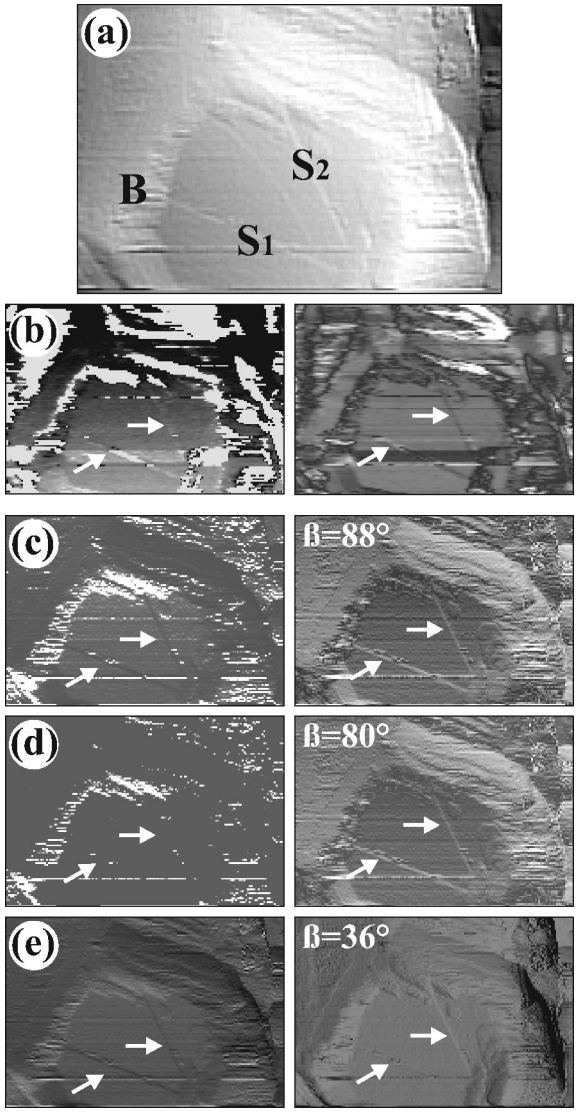

FIG. 2. (a) $62\times42\ \mathrm{nm}^2$ topview of a 100-nm-thick Au film on Y-cut $LiNbO_3$ as well as (b) phase (left) and amplitude (right) images of a HVP–SAW, all recorded simultaneously with the SAW–STM. (c)–(e) Simulated phase (left) and amplitude images (right) at different angles β of the oscillation ellipse. Good agreement with experiment is achieved with $\beta=88°$.

Here $g_x=(\tan\gamma_x)^2$ and $g_y=(\tan\gamma_y)^2$ account for the local tilt that is given by the inclination angles γ_x and γ_y, respectively. β denotes the eccentricity angle of the oscillation ellipse and is calculated by $\beta=\arctan(u_1/u_3)$ from the respective longitudinal and transverse displacement amplitudes u_1 and u_3 ($u_0=\sqrt{u_1^2+u_3^2}$). Note that because of the derivatives occurring in Eqs. (1) and (2), the structural features are even more pronounced in amplitude and phase images compared with topography.

Comparison of the experimental results with phase and amplitude images simulated by Eqs. (1) and (2) enables the quantitative determination of the eccentricity β of the SAW oscillation ellipse. Figures 2(c)–2(e) show simulations for different values of β using the experimental topography [Fig. 2(a)] as input parameter. Obviously, the best agreement with experiment is achieved with β close to the theoretical value $\beta_{th}=88°$ for the HVP–SAW on Y-cut $LiNbO_3$. The influence of topography is reproduced on a quantitative level for structural features with dimensions above 1–2 nm. This concerns, for instance, the increase of phase (bright) or the re-

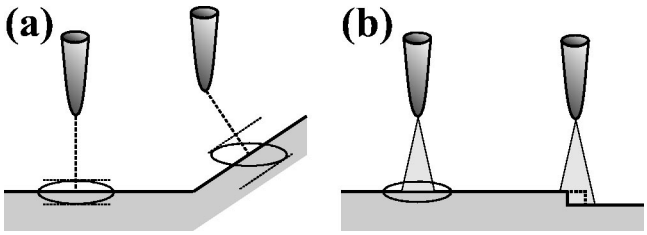

FIG. 3. Schematic illustration of the SAW detection by a SAW–STM: (a) on facets that larger than the tunneling regime, where Eqs. (1) and (2) apply, and (b) at a step of single height, which lies inside the (shaded) tunneling regime.

duced amplitude (dark) at the inclined border compared with the interior of the horizontal plateau. For $\beta = 80°$ the agreement with experiment is significantly decreased, pointing to an experimental accuracy of about $\pm 5°$. Note that the respective amplitude contrast is even inversed for $\beta = 36°$, i.e., the value of the Rayleigh wave [Fig. 2(e)].

In addition, the experimental results of Fig. 2 indicate a breakdown of the current model once the feature sizes approache atomic dimensions. In fact, the two single steps S_1 and S_2 resolved in Fig. 2(a) are imaged with opposite contrast compared with the simulated phase and amplitude images [e.g., Figs. 2(c)–2(e)]. In the model of Chilla *et al.*,[6,13] it is assumed that tunneling proceeds from facets with dimensions exceeding the typical area from which the (majority of the) tunneling current is collected ($\sim 1 \times 1\ \mathrm{nm}^2$). As illustrated in Fig. 3(a), in that case the STM tip probes amplitude and phase of the geometrical projection of the oscillation ellipse according to Eqs. (1) and (2).

A different situation is encountered when the feature of interest lies inside the tunneling regime. Figure 3(b) compares tunneling from a horizontal terrace and close to a step edge. As long as the tip scans the terrace [Fig. 3(b), left], mainly the vertical oscillation component is detected; the in-plane oscillation of the SAW is not accompanied by a change in the overall tunneling current. At a step [Fig. 3(b), right] the upper terrace dominates the tunneling current due to the exponential decay with distance. The lateral oscillation of the SAW periodically increases and decreases the fraction of the current tunneling from upper terrace, thus giving rise to an additional modulation of tunneling current; note that its phase is shifted by $\pi/2$ against the vertical component.

Estimation of the mixing signal ($I_{\Delta\omega}$) measured by an atomically sharp STM tip on the terrace (T) and at a step edge (S) yields the following expression:

$$\frac{I_{\Delta\omega,S}}{I_{\Delta\omega,T}} \approx \frac{\kappa_S}{\kappa_T} \frac{\frac{1}{2}\left[\cos(\Delta\omega t) - \frac{u_1}{u_3}\frac{1}{\sqrt{\kappa_S \pi d_0}}\sin(\Delta\omega t)\right]}{\cos(\Delta\omega t)}. \quad (3)$$

With typical values for the tunneling distance ($d_0 = 1$ nm), the surface oscillation ($u_1 = 0.05$ nm and $u_3 = 0.00175$ nm, corresponding to $\beta = 88°$), the reciprocal decay length of the terrace ($\kappa_T = 0.01$ nm), and a decreased work function[14] at the step edge by 25% modifying κ_S appropriately, the amplitude of the mixing signal at the step is by a factor of 2.2 larger than on the terrace contrary to experiment; the corresponding phase is 79°. A more detailed analysis reveals that the relative contribution of the lateral oscillation to the total signal depends strongly on the shape of the STM tip. Since the collection area for the tunneling is increased with more rounded tips, the lateral step movement contributes less to the total tunneling current and reduced amplitudes may be observed at steps. For a flat tip with an apex of about 2 nm the amplitude at a step is already smaller compared with the terrace and accordingly there is only a very small phase change. We remark that a tip apex of about 2 nm can be deduced from the step width measured in the topography of Fig. 2(a).

In conclusion, our study demonstrates that UHV SAW–STM is indeed a powerful nanoscale probe for identification of SAWs and for investigation of SAWs with even negligible out-of-plane components. Whereas phase and amplitude images are properly described by the model of Chilla *et al.*[6,13] on extended facets, both the tip geometry and the local surface movement have to be treated in more detail once the feature size reaches atomic dimensions. As revealed by our analysis, also the mixing signal measured at a step edge contains information about the eccentricity, and thus of the ratio u_1/u_3 of the surface oscillation. Since u_1/u_3 is directly related to the elastic constants, the latter result is particulary promising for future studies of nanoscale elasticity.

The authors wish to thank S. Krauß for technical support, W. Seidel for providing the IDT samples, E. Chilla for helpful discussions, and P. Santos for carefully reading the manuscript. The work was sponsored by the European Union (EFRE).

[1] P. Hess, Phys. Today **55**, 42 (2002).
[2] D. Royer and E. Dieulesaint, *Elastic Waves in Solids I* (Springer, Berlin, 2000).
[3] S. Zimmermann, A. Wixforth, J. P. Kotthaus, W. Wegscheider, and M. Bichler Science **283**, 1292 (1999).
[4] O. V. Kolosov, M. R. Castell, C. D. Marsh, G. A. D. Briggs, T. I. Kamins, and R. S. Williams, Phys. Rev. Lett. **81**, 1046 (1998).
[5] T. Sogowa, P. Santos, S. K. Zhang, S. Eshlagi, A. D. Wieck, and K. H. Ploog, Phys. Rev. Lett. **87**, 276601 (2001).
[6] E. Chilla, W. Rohrbeck, H.-J. Fröhlich, R. Koch, and K. H. Rieder, Appl. Phys. Lett. **61**, 3107 (1992).
[7] T. Hesjedal, E. Chilla, and H.-J. Fröhlich, Appl. Phys. Lett. **69**, 354 (1996).
[8] J.-P. Monchalin, IEEE Trans. Ultrason. Ferroelectr. Freq. Control **UFFC-33**, 485 (1986),
[9] G. Behme, T. Hesjedal, E. Chilla, and H.-J. Fröhlich, Appl. Phys. Lett. **73**, 882 (1998).
[10] P. U. Voigt, S. Krauß, E. Chilla, and R. Koch, J. Vac. Sci. Technol. A **19**, 1817 (2001).
[11] R. Koch, D. Winau, A. Führmann, and K. H. Rieder, Vacuum **43**, 521 (1992).
[12] P. U. Voigt and R. Koch, J. Appl. Phys. **92**, 7160 (2002).
[13] E. Chilla, W. Rohrbeck, H.-J. Fröhlich, R. Koch, and K. H. Rieder, Ann. Phys. **3**, 21 (1994).
[14] J. F. Jia, K. Inoue, Y. Hasegawa, W. S. Yang, and T. Sakurai, Phys. Rev. B **58**, 1193 (1998).